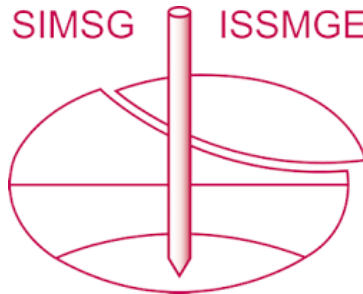


INTERNATIONAL SOCIETY FOR SOIL MECHANICS AND GEOTECHNICAL ENGINEERING



This paper was downloaded from the Online Library of the International Society for Soil Mechanics and Geotechnical Engineering (ISSMGE). The library is available here:

<https://www.issmge.org/publications/online-library>

This is an open-access database that archives thousands of papers published under the Auspices of the ISSMGE and maintained by the Innovation and Development Committee of ISSMGE.

The paper was published in the proceedings of the 10th European Conference on Numerical Methods in Geotechnical Engineering and was edited by Lidija Zdravkovic, Stavroula Kontoe, Aikaterini Tsiampousi and David Taborda. The conference was held from June 26th to June 28th 2023 at the Imperial College London, United Kingdom.

To see the complete list of papers in the proceedings visit the link below:

<https://issmge.org/files/NUMGE2023-Preface.pdf>

On the calibration and application of the NorSand model

E. Castillo-Fuentes¹, L. Zdravkovic¹, D.M. Potts¹

¹*Department of Civil and Environmental Engineering, Imperial College London, UK*

ABSTRACT: Advanced constitutive models that are capable of reproducing different aspects of sand behaviour have been an object of study for many years. The models developed in the critical state soil mechanics framework, with a formulation based on the state parameter, are of particular interest as they can predict the sand response over a full range of stresses and void ratios. This paper briefly introduces a generalised 3D formulation of the NorSand constitutive model, as one of the models with such capabilities. The model is attractive for use due to its relative simplicity and a small number of model parameters that can be obtained from conventional laboratory testing. The calibration of the model presents and discusses the process of integrating laboratory and field data on the example of natural Dunkirk sand. The performance of the model is finally validated in the finite element analysis of a laterally loaded pile, by favourable comparison of numerical results against field measurements of pile response to lateral loading.

Keywords: Finite element; Constitutive modelling; Sand behaviour; NorSand.

1 INTRODUCTION

The use of advanced numerical tools, such as the finite element (FE) method, in the solution of geotechnical problems is widespread in research and practice nowadays. The accuracy of a FE analysis relies on a number of factors, a critical one being the choice of an appropriate constitutive model that allows the reproduction of key aspects of soil behaviour that are important for a specific problem. To model the mechanical response of granular materials simple Mohr-Coulomb type models have been used frequently, while more recently models based on critical state soil mechanics (CSSM) and state parameter frameworks have been implemented in FE codes. The latter models are capable of reproducing advanced aspects of sand behaviour, such as stress and void ratio dependency of stiffness and strength, anisotropy, or energy dissipation upon cyclic loading, with a single set of model parameters. However, they often require a large number of input parameter, hence their calibration may involve a lengthy and complex process.

In contrast, the former models usually require a smaller set of input parameters that can be derived more directly from experimental data but are limited in the realistic representation of the sand response, often related only to a particular level of stress or relative density. Consequently, different sets of model parameters may be required to address a realistic boundary value problem.

Examples of state parameter CSSM sand models that are frequently used and written about include a series of bounding surface plasticity (BSP) models (e.g., Manzari and Dafalias, 1997; Loukidis and Salgado 2008; Taborda et al., 2014) and the NorSand model (Jefferies,

1993; Jefferies and Been, 2015), the latter being the focus of this paper. The NorSand constitutive model has as a basis the formulation of the original critical state Cam Clay model (Schofield and Wroth, 1968), but introduces, importantly, the state parameter framework of Been and Jefferies (1985).

This paper presents the main aspects of a generalised 3D formulation of the NorSand constitutive model, as implemented in the FE software ICFEP (Potts and Zdravkovic, 1999, 2001). The model calibration is then presented and its capabilities examined on a 3D FE simulation of a monopile foundation under the conditions of monotonic loading.

2 NORSAND MODEL FORMULATION

The model is generalised in the $J - p' - \theta$ space, where J is the generalised deviatoric stress invariant, p' is the mean effective stress and θ is the Lode's angle (see e.g. Potts and Zdravkovic (1999) for definitions of invariants). The adopted sign convention is compression positive and this version of the model does not account for cyclic loading.

2.1 Elasticity

The elasticity of the model is defined by the shear stiffness and Poisson's ratio, ν . The shear modulus, G_{max} , is expressed as a function of the mean effective stress, p' :

$$G_{max} = G_{ref} \cdot \left(\frac{p'}{p'_{ref}} \right)^m \quad (1)$$

where G_{ref} is the shear modulus at reference pressure, p'_{ref} , and m is a material parameter with a typical value of around 0.5 (Jefferies and Been, 2015).

2.2 Plasticity

The hardening parameter of the model is evaluated at the image point (Figure 1), defined as a point at which the derivative of the yield surface $dF/dp' = 0$. An associated flow rule applies in the $J - p'$ plane and a non-associated flow rule in the deviatoric plane.

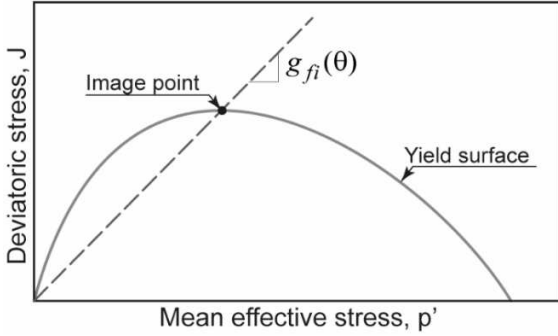


Figure 1. Yield surface and location of the image point in the $J - p'$ plane.

2.2.1 Critical state line (CSL)

The model introduces the concept of state parameter, ψ , defined as:

$$\psi = e - e_{cs} \quad (2)$$

where e is the current void ratio and e_{cs} is the critical state void ratio for the same magnitude of p' .

The shape of the CSL in the $e - \ln p'$ space can be linear, Equation (3a), or curved, Equation (3b):

$$e_{cs} = e_{cs.ref} - \lambda \cdot \ln\left(\frac{p'}{p'_{ref}}\right) \quad (3a)$$

$$e_{cs} = e_{cs.ref} - \lambda \cdot \left(\frac{p'}{p'_{ref}}\right)^\xi \quad (3b)$$

where $e_{cs.ref}$ is the void ratio at the reference pressure, p'_{ref} , while λ and ξ are a model parameters.

2.2.2 Yield surface

The yield surface, F , is defined as:

$$F = \frac{J}{p' g_{fi}(\theta)} - \left(1 + \ln\left(\frac{p'_i}{p'}\right)\right) = 0 \quad (4)$$

where p'_i is the mean effective stress at the image point and $g_{fi}(\theta)$ is given as:

$$g_{fi}(\theta) = g_{f,cs}(\theta) \cdot \left(1 - \frac{N\chi|\psi_i|}{g_{f,cs}(\theta = -30^\circ)}\right) \quad (5)$$

In the above, $g_{f,cs}(\theta)$ is the gradient of the critical state line in the $J - p'$ plane and $g_{f,cs}(\theta = -30^\circ)$ is its value in triaxial compression (at $\theta = -30^\circ$):

$$g_{f,cs}(\theta) = \frac{\sin\phi'}{\cos\theta + \frac{\sin\theta\sin\phi'}{\sqrt{3}}} \quad (6)$$

N is a coupling volumetric parameter and χ is a material parameter relating the maximum dilatancy, $D_{p,max} = (d\varepsilon_{vol}^{pl}/dE_d^{pl})_{max}$, and the state parameter at the image point, ψ_i , as $D_{p,max} = \chi\psi_i$. From the definition of plastic dilatancy, D_p , and the yield surface in Equation (4) the following stress-dilatancy relationship is obtained:

$$D_p = g_{fi}(\theta) - \frac{J}{p'} \quad (7)$$

2.2.3 Plastic potential surface

The plastic potential surface has a form similar to Equation (4):

$$P = \frac{J}{p' g_{pi}(\theta)} - \left(1 + \ln\left(\frac{p'_i}{p'}\right)\right) = 0 \quad (8)$$

where $g_{pi}(\theta)$ is a function similar to Equation (5), but with $g_{f,cs}(\theta)$ and $g_{f,cs}(\theta = -30^\circ)$ replaced by $g_{p,cs}(\theta)$ and $g_{p,cs}(\theta = -30^\circ)$, respectively.

2.2.4 Hardening rule

The hardening rule is expressed as a proportion of the difference in p' between the image point at maximum dilatancy ($D_{p,max}$) and the current stress image point:

$$dp'_i = \left(H \frac{p'}{p'_i} \frac{g_{pi}(\theta)}{g_{pi}(\theta = -30^\circ)} (p'_{i,max} - p'_i) - S\right) \cdot dE_d^{pl} \quad (9)$$

where S is a parameter that enables the reproduction of additional softening and, hence, a more realistic behaviour of loose sands in undrained loading. H is the hardening modulus defined as a linear function of the state parameter as $H = H_0 + H_\psi \cdot \psi$, where H_0 and H_ψ are model parameters.

3 CALIBRATION OF THE MODEL

The calibration of the NorSand model is carried out on the example of Dunkirk sand, as a natural marine sand in northern France. Jefferies and Shuttle (2005) recommend five triaxial compression tests to be used for calibration, noting three tests to be a bare minimum.

The calibration is based on the experimental data presented in Zdravkovic et al. (2020) and Taborda et al.

(2020), used in those references for the calibration of a BSP model. The applied process is hierarchical, calibrating first the parameters that can be derived directly from test data. The remaining parameters are then varied iteratively in simulations of element tests and their values are estimated from the best agreement between simulated and measured experimental response of Dunkirk sand.

3.1 Elasticity

The parameters G_{ref} , p'_{ref} and m from Equation (1) are estimated by the best fit to the data shown in Figure 2. In this case $p'_{ref} = 101.3$ kPa is the atmospheric pressure. The laboratory data from isotropically consolidated drained triaxial compression tests of Liu (2018), reporting the measurements of the vertical Young's modulus, E_v , were utilised in conjunction with a Poisson's ratio $\nu = 0.17$ (Kuwano, 1999) to evaluate the G_{max} at different stress levels. The best fit equation in the figure implies $G_{ref} = 100$ MPa and $m = 0.5$.

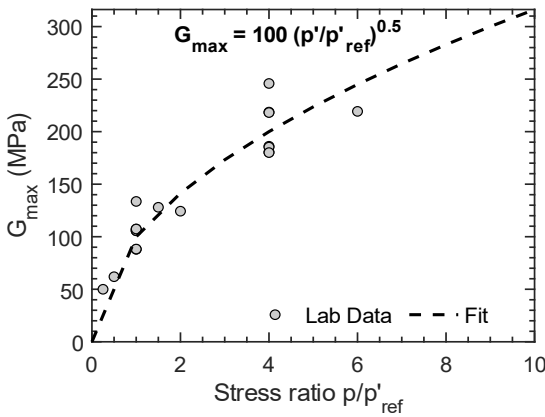


Figure 2. Calibration of elastic stiffness from triaxial tests.

3.2 CSL

The CSL in the $e - \ln p'/p'_{ref}$ plane (Figure 3) is fitted primarily to anisotropically consolidated drained triaxial compression tests (Aghakouchak, 2015) presented in Zdravkovic et al. (2020), although the figure also shows the Liu (2018) data. The initial void ratio in most of the tests was $e_0 = 0.64$, corresponding to the state of natural Dunkirk sand and its relative density, D_R , of 75%. One test was set up at $e_0 = 0.59$, corresponding to $D_R \sim 100\%$. The initial confinement pressures varied from 50 kPa to 400 kPa.

The parameter $e_{cs,ref} = 0.91$ in this case is set equal to the maximum void ratio of Dunkirk sand (Zdravkovic et al., 2020), at $p' = 0$ kPa. The parameters λ and ξ are derived by assuming a curved CSL and using the least-square method through Aghakouchak (2015) data, resulting in $\lambda = 0.135$ and $\xi = 0.18$.

For the estimation of $g_{f,cs}(\theta)$ in Equation (6), it is critical to determine the maximum stress ratio in triaxial compression, M_{tc} , as a gradient of CSL in the $q - p'$

plane. The difficulty in determining the critical state in triaxial testing of sands is widely recognised and Jefferies and Shuttle (2005) suggest that this limitation may result in M_{tc} being estimated at test stages earlier than the critical state. Figure 4 shows the suggested linear relationship between the stress ratio, η_{max} , at maximum dilatancy, and the value of maximum dilatancy, $D_{p,max}$, for each triaxial test used in this calibration, using the expression presented in Equation (7). This results in values of $1 - N = 0.8$ (hence $N = 0.2$) and $M_{tc} = 1.3$, the latter implying the value of the angle of shearing resistance in triaxial compression $\phi'_{tc} = 32^\circ$.

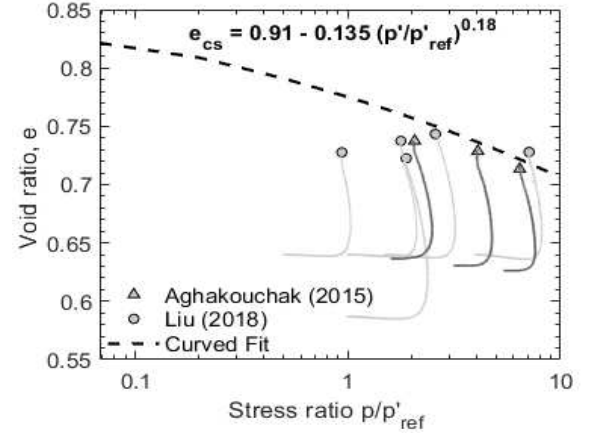


Figure 3. Definition of the CSL in the $e - \ln p'/p'_{ref}$ plane for Dunkirk sand.

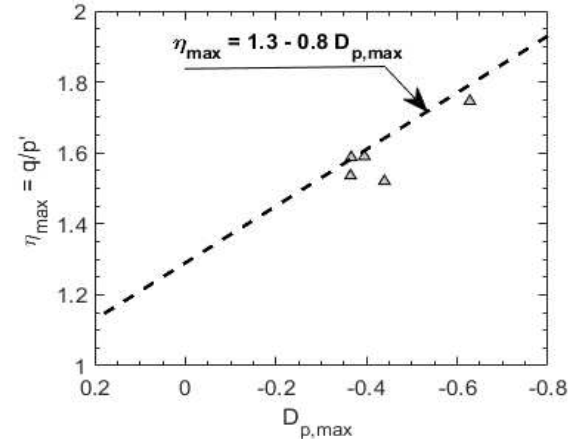


Figure 4. Determination of M_{tc} (ϕ'_{cs}) and N .

3.3 Plastic behaviour

The plastic behaviour in the model is controlled by the parameters χ and H , as shown in Equations (5) and (9). The former parameter is estimated from the relationship between the maximum dilatancy, $D_{p,max}$ and the state parameter, ψ , at that point. A linear fitting between these variables, as shown in Figure 5, results in the gradient equivalent to the parameter $\chi = 2.6$.

The hardening modulus, H , is obtained from an iterative process, where the parameter H_0 is varied to produce the best simulation of each triaxial test separately, with H_ψ assumed as zero. In this case, one value of H_0

is obtained for each test, and the final value is estimated from the resulting trend against the initial state parameter, ψ_{ini} , with $H(\psi) = H_0 + H_\psi \cdot \psi$. Jefferies and Been (2015) propose an initial guess value for H_0 of $4/\lambda$, which in the current case is around 30.

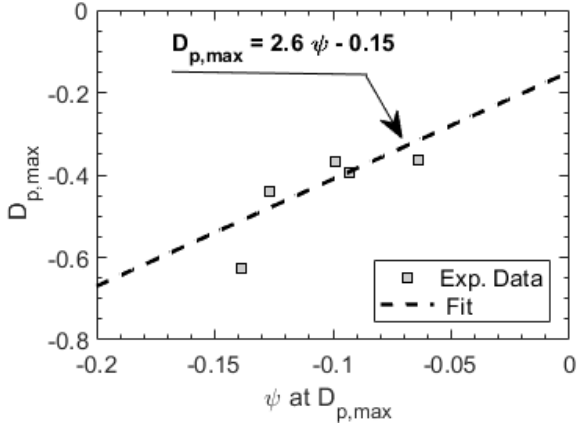


Figure 5. Calibration of the plastic parameter χ .

Figure 6 shows the effect of H_0 in the simulated stress-strain curves for one of the tests ($e_0 = 0.64$, $p'_0 = 150\text{kPa}$), compared against the experimental data. From the five triaxial tests calibrated independently, the most appropriate value for H_0 is 92.0, giving on average the best simulation for each test.

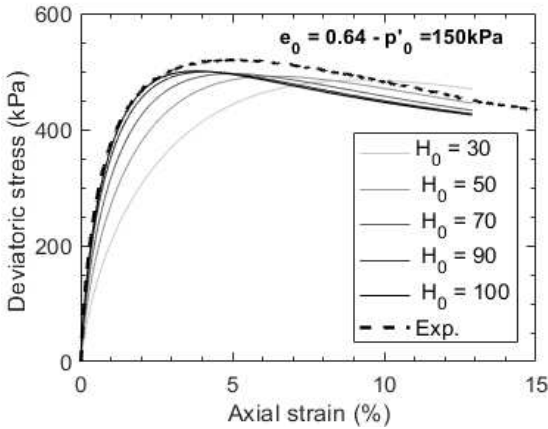


Figure 6. Adjustment of the model parameter H .

3.4 Integration of field tests into calibration

The calibration process so far ensures that derived model parameters reproduce very closely the deviatoric stress-axial strain and volumetric strain-axial strain behaviour measured in triaxial tests used in the calibration process. However, the field tests in Dunkirk sand, in particular the seismic cone penetration tests (SCPTs) in Figure 7, have shown a substantially larger values of the elastic shear modulus, G_{max} , compared to those derived from local instruments attached to triaxial specimens in laboratory testing (Figure 7). This was explained by a potentially low resolution of local devices to measure the real elastic stiffness. As a result, the next stage of the calibration process involves adjustment of model parameters to reproduce the field values of G_{max} , while

maintaining the same peak and ultimate strength measured in triaxial tests. A similar approach was applied in the calibration of a BSP model, Taborda et al. (2020).

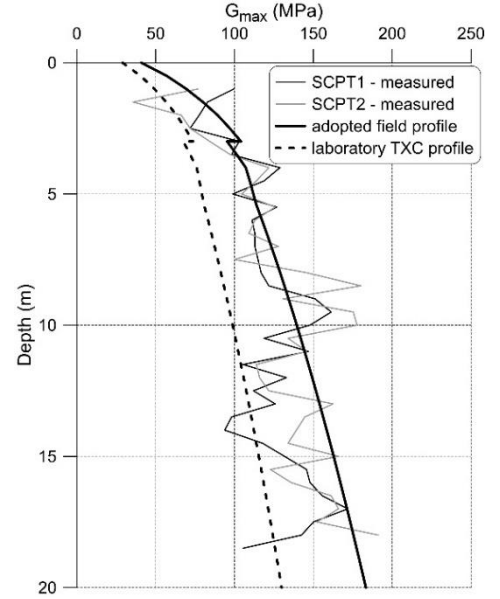


Figure 7. Field and laboratory G_{max} profiles at Dunkirk

Based on Equation (1), the G_{ref} parameter may seem an obvious one to increase in order to increase the G_{max} . However, changing this alone does not produce the expected stiffening of the stress-strain curve, compared to the original calibration (Figure 8). This is explained by the fact that the elastic parameter change affects the very small strain range, while the majority of the stress-strain curve engaging plasticity. Consequently, the tangent modulus, $G_{tan} = \delta J / \delta E_d$, and hence the shape of the stress-strain curve, depends on additional parameters. The expression for the tangent modulus, G_{tan} , considering the hardening rule in Equation (9), reveals the dependency on the hardening parameter H :

$$G_{tan} = \frac{\delta J \cdot G_{max} H \frac{p'_i}{p'} \widetilde{g}_{pi}(p'_{i,max} - p'_i)}{\delta J \cdot H \frac{p'_i}{p'} \widetilde{g}_{pi}(p'_{i,max} - p'_i) + \delta p'_i G_{max}} \quad (10)$$

where $\widetilde{g}_{pi} = g_{pi}(\theta) / g_{pi}(\theta = -30^\circ)$.

Consequently, in order to fit the field data, the adjustment of both G_{ref} and H parameters needs to be conducted. Figures 8 and 9 show, respectively, the resulting deviatoric stress-axial strain and volumetric strain-axial strain curves for the same test with $e_0 = 0.64$ and $p'_0 = 150\text{ kPa}$, compared against the initial calibration from Figure 6. The marginal effect of G_{ref} is demonstrated in the figures, while the additional modification of H shows a clear stiffening of the stress-strain curve, while maintaining similar peak and ultimate strengths. This adjustment of the model parameters was conducted for all the available tests and the final model parameters are summarised in Table 1.

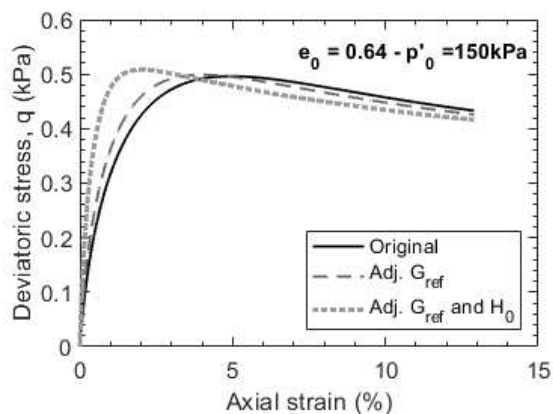


Figure 8. Adjustment of model parameters to fit in-situ shear modulus: comparison of stress-strain curves.

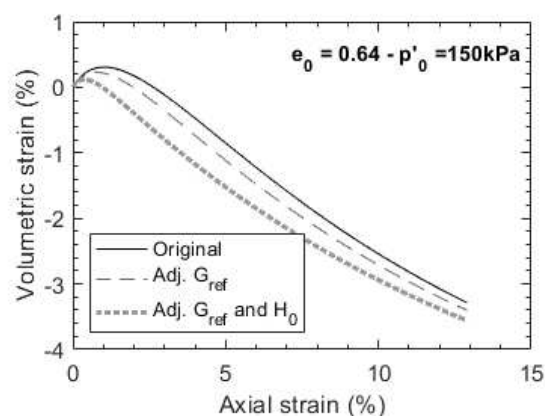


Figure 9. Adjustment of model parameters to fit in-situ shear modulus: comparison of volumetric strain curves.

Table 1. Summary of NorSand parameters for Dunkirk sand.

Parameter	Dunkirk Sand
$\lambda(-)$	0.135
$e_{cs,ref}(-)$	0.910
p'_{ref} (kPa)	101.3
$\phi'(^{\circ})$	32.0
N	0.2
H_0 (-)	230.9
H_{ψ} (-)	0.0
G_{ref} (MPa)	150.0
m (-)	0.5
ν (-)	0.17

4 VALIDATION IN A BOUNDARY VALUE PROBLEM

The performance of the calibrated NorSand model is examined in a 3D FE analysis of one of the pile tests in Dunkirk sand, conducted for the PISA project (McAdam et al., 2020). The results are compared against the field measurements and against their interpretation with the optimised structural model of Burd et al. (2020).

The geometry and a FE mesh of the model are shown in Figure 10. The steel tubular pile has a diameter $D =$

2.0 m and an embedded length, $L = 10.5$ m. The pile is loaded laterally with a force H , applied at $h = 10.0$ m eccentricity from the ground surface. The initial stresses and boundary conditions are identical to the analysis of this pile presented in Taborda et al. (2020), using a BSP constitutive model.

Figure 11 shows a favourable comparison between the computed and measured monotonic horizontal load and horizontal ground level displacement (the latter measured on the passive side of the pile). Figure 12 further compares the behaviour of the embedded part of the pile in terms of its deflected shape and bending moment profiles at early and late stages of loading. Good agreement is seen between measurements and analysis results, demonstrating the ability of the numerical model to capture accurately the early-stage flexure of the pile and its late stage rigid body response.

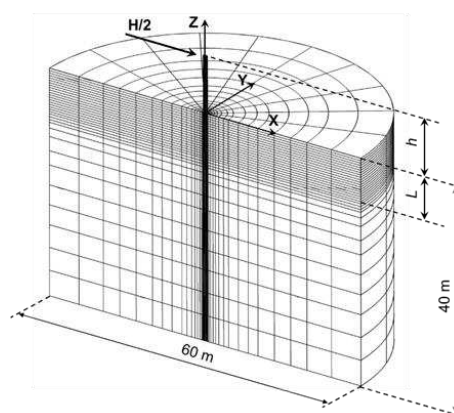


Figure 10. Geometry and FE mesh of analysed pile.

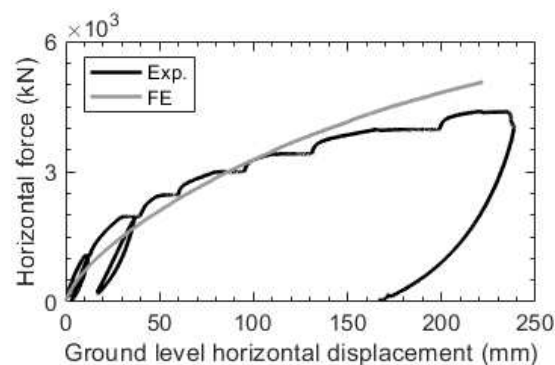


Figure 11. Horizontal force versus ground level horizontal movement (data after McAdam et al., 2020)

5 CONCLUSIONS

The paper has introduced the main aspects of a 3D generalised formulation for the NorSand constitutive model, as adopted in the FE code ICFEP. The main feature of the model is its reasonably straightforward calibration and a small number of input parameters. The paper has presented a successful model calibration process on the example of Dunkirk sand. The calibration is hierarchical, deriving first the parameters that can be determined directly from experimental data, followed by parameters that require a numerical iterative process.

The paper also shows integration of laboratory and field data to reproduce realistic soil stiffness, emphasising the need to combine both the elastic shear modulus and the plastic hardening modulus of the model to achieve this.

The model performance is validated on a simulation of a laterally loaded pile test in dense Dunkirk sand. The results show a very good agreement between model predictions and measured pile response.

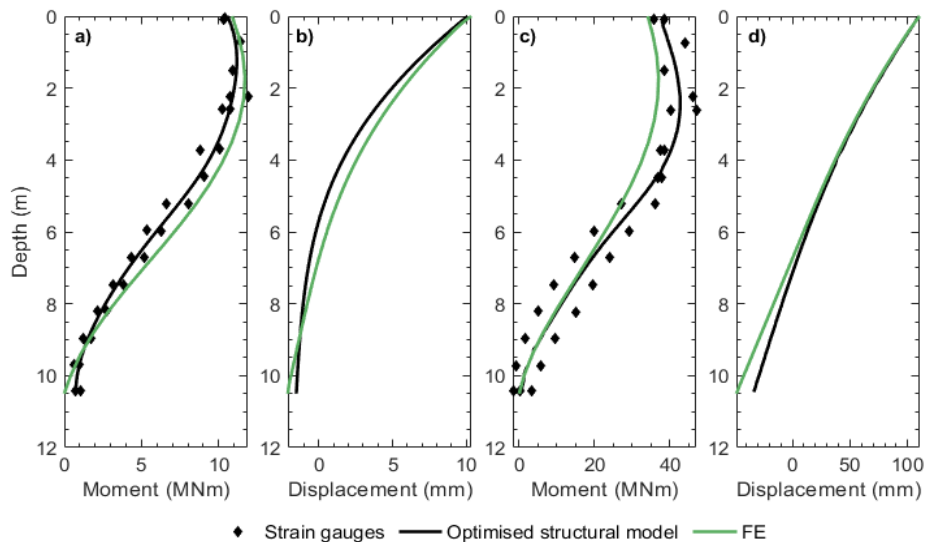


Figure 12. Comparison of field measurements and FE predictions, for the ground level: a) moment of 10.8 MNm, b) horizontal displacement of 10.1 mm, c) moment of 34.1 MNm and c) horizontal displacement of 110.1 mm (data after McAdam et al., 2020).

7 REFERENCES

- Aghakouchak, A., 2015. *Advanced laboratory studies to explore the axial cyclic behaviour of driven piles*. PhD Thesis, Imperial College London
- Been, K., Jefferies, M.G., 1985. A state parameter for sands. *Géotechnique* **35**, 99–112.
- Burd, H.J., Taborda, D.M.G., Zdravković, L., Abadie, C.N., Byrne, B.W., Houlsby, G.T., Gavin, K.G., Igoe, D.J.P., Jardine, R.J., Martin, C.M., McAdam, R.A., Pedro, A.M.G., Potts, D.M., 2020. PISA design model for monopiles for offshore wind turbines: application to a marine sand. *Géotechnique* **70**, 1048–1066.
- Jefferies, M., Been, K., 2015. *Soil Liquefaction: A Critical State Approach*, Second Edition, CRC Press.
- Jefferies, M.G., 1993. Nor-Sand: a simple critical state model for sand. *Géotechnique* **43**, 91–103.
- Jefferies, M.G., Shuttle, D.A., 2005. NorSand: Features, Calibration and Use, in: *Soil Constitutive Models*. Presented at the *Geo-Frontiers Congress 2005*, American Society of Civil Engineers, Austin, Texas, United States, 169, 204–236.
- Kuwano, R., 1999. *The stiffness and yielding anisotropy of sand*. PhD Thesis, Imperial College London
- Liu, T., 2018. *Advanced laboratory testing for offshore pile foundations under monotonic and cyclic loading*. PhD Thesis, Imperial College London
- Loukidis, D., Salgado, R., 2009. Modelling sand response using two-surface plasticity. *Computers and Geotechnics* **36**, 166–186.
- Manzari, M.T., Dafalias, Y.F., 1997. A critical state two-surface plasticity model for sands. *Géotechnique* **47**, 255–272.
- McAdam, R.A., Byrne, B.W., Houlsby, G.T., Beuckelaers, W.J.A.P., Burd, H.J., Gavin, K.G., Igoe, D.J.P., Jardine, R.J., Martin, C.M., Muir Wood, A., Potts, D.M., Skov Gretlund, J., Taborda, D.M.G., Zdravković, L., 2020. Monotonic laterally loaded pile testing in a dense marine sand at Dunkirk. *Géotechnique* **70**, 986–998.
- Potts, D.M., Zdravković, L., 1999. *Finite Element Analysis in Geotechnical Engineering: Theory*. Thomas Telford Publishing.
- Potts, D.M., Zdravković, L., 2001. *Finite Element Analysis in Geotechnical Engineering: Application*. Thomas Telford Publishing.
- Schofield, A.N., Wroth, P. 1968. *Critical state soil mechanics*. McGraw Hill.
- Taborda, D.M.G., Zdravković, L., Kontoe, S., Potts, D.M., 2014. Computational study on the modification of a bounding surface plasticity model for sands. *Computers and Geotechnics* **59**, 145–160.
- Taborda, D.M.G., Zdravković, L., Potts, D.M., Burd, H.J., Byrne, B.W., Gavin, K.G., Houlsby, G.T., Jardine, R.J., Liu, T., Martin, C.M., McAdam, R.A., 2020. Finite-element modelling of laterally loaded piles in a dense marine sand at Dunkirk. *Géotechnique* **70**, 1014–1029.
- Zdravković, L., Jardine, R.J., Taborda, D.M.G., Abadias, D., Burd, H.J., Byrne, B.W., Gavin, K.G., Houlsby, G.T., Igoe, D.J.P., Liu, T., Martin, C.M., McAdam, R.A., Muir Wood, A., Potts, D.M., Skov Gretlund, J., Ushev, E., 2020. Ground characterisation for PISA pile testing and analysis. *Géotechnique* **70**, 945–960.

6 ACKNOWLEDGEMENTS

The authors would like to acknowledge the sponsorship for the PhD research of the first author provided by the National Research and Development Agency (ANID) from Chile and by the Dixon Scholarship from the Department of Civil and Environmental Engineering at Imperial College.